Nanomed Res J 11(3):262-273, Summer 2026

RESEARCH ARTICLE

Morphine Antibody Conjugated SiO_2@Au Core-Shell Nanoparticles: Synthesis, Characterization, and Application in Colorimetric Detection

Asmau Sahabi Mukhtar[1], Zoha Babaei Afrapoli[1,2], Sharmin Kharrazi[1*], Reza Faridi-Majidi[1*]

[1] Department of Medical Nanotechnology, School of Advanced Technologies in Medicine, Tehran University of Medical Sciences (TUMS), Tehran, Iran.

[2] Department of Medical Nanotechnology, School of Advanced Technologies in Medicine, Mazandaran University of Medical Sciences, Sari, Iran.

ARTICLE INFO

Article History:
Received: 2026-02-10
Revised: 2026-05-10
Accepted: 2026-05-18

Keywords:
Core-Shell Nanoparticles
Bioconjugation
Morphine Antibody
Colorimetric Detection

ABSTRACT

The global opioid crisis, particularly the abuse of drugs like morphine is a massive public health challenge that demands faster, better detection methods and innovative technologies like core-shell nanoparticle (CS NPs) biosensors for fast and efficient monitoring and treatment. This study aimed to develop a rapid and simple method for synthesizing SiO_2@Au CS NPs and functionalizing their surface by attaching a morphine antibody as a model analyte for colorimetric detection. SiO_2@Au CS NPs was synthesized using an iterative hydroxylamine seeding method and characterized through various techniques, including UV-visible spectroscopy, dynamic light scattering (DLS), scanning electron microscope (SEM), energy-dispersive X-ray analysis (EDX), dot-blot assay, and Bradford. SEM and DLS analyses demonstrated that both SiO_2 NPs and SiO_2@Au CS NPs exhibited spherical shapes with uniform size distributions (178 nm and 182 nm) and average diameters of 226 ± 2 nm and 291 ± 5 nm, respectively. EDX analysis verified the elemental composition of both the bare silica and CS NPs. The effective conjugation of bare silica with gold, facilitated by hydroxylamine as a linker, was successfully observed in the CS NPs. Furthermore, the Bradford assay indicated that the nanoparticle surface displayed a high antibody-binding efficiency of approximately 99%. The Dot blot assay provided visible results within 3-4 minutes. The findings of this study confirmed that antibody-conjugated SiO_2@Au CS NPs proved to be effective as bioprobes in dot blot assays. The integration of multiple materials for biomolecule attachment demonstrated greater efficiency than single-material approaches, leading to enhanced visibility in colorimetric detection applications.

How to cite this article
Sahabi Mukhtar A, Babaei Afrapoli Z, Kharrazi Sh, Faridi-Majidi R. Morphine Antibody Conjugated SiO_2@Au Core-Shell Nanoparticles: Synthesis, Characterization, and Application in Colorimetric Detection. Nanomed Res J, 2026; 11(3): 262-273.
DOI: 10.22034/nmrj.2026.03.006

INTRODUCTION

Opioid abuse epidemics have been prevalent in recent years and have become a significant global health concern. Stimulants such as morphine, codeine, and fentanyl are the most abused drugs and deadliest drug type, they possess analgesic and sedative effects which are normally used for pain relief [1]. However, non-medical use, prolonged use, misuse, and use without medical supervision of morphine can lead to health problems, such as respiratory depression, addiction, constipation, dizziness, and confusion. [2]. According to the World Drug Report (2022), it was estimated that nearly 61 million cases have opioid abuse [3]. In the United States, 500,000 deaths were ascribable to opioid overdoses from 1999 to 2019 due to regularly prescribed and illegally acquired drugs [4]. Therefore, the detection of morphine levels in biological samples such as urine and blood can assist in identifying the causes of death in clinical

* Corresponding Author Email: *refaridi@tums.ac.ir*
sh-kharrazi@tums.ac.ir

This work is licensed under the Creative Commons Attribution 4.0 International License.
To view a copy of this license, visit http://creativecommons.org/licenses/by/4.0/.

cases, managing abuse, and monitoring the level of treatment [5].

Conventional and point-of-care (POC) testing are used to detect morphine. POC offers rapid and convenient on-site testing without the need for specialized laboratory facilities, whereas conventional methods require longer time to generate results [6]. One promising technology for clinical and personalized POC diagnostics is colorimetric sensing of target analytes because of its optical properties, low cost, and simplicity of detection [7]. Gold nanoparticles (Au NPs) have been introduced into colorimetric sensing systems owing to their stability and visible spectrum [1, 8]. In recent years, it has become increasingly clear that multiphase nanoparticles, such as CS NPs, exhibit superior properties and efficiency compared to single-phase nanoparticles (SP NPs) [9-11]. One of the most widely used CS NPs is silica-gold (SiO_2@Au) CS NPs, which have drawn significant attention from researchers because of their unique properties, such as low toxicity, high stability, enhanced mechanical and thermal stability of silica, and the catalytic, electrical, and optical properties of gold [12-16].

Recent research has highlighted the influence of CS NPs on their distinctive properties compared to SP NPs. For example, studies have shown that substituting SP NPs (gold NPs) with CS NPs (SiO_2@Au) in SERS substrates results in a better electric field distribution and absorption cross-section. Moreover, the SERS enhancement factor was approximately twice that of SP NPs [17]. Other studies have shown that the detection of Pb^{2+} ions using SiO_2@Au CS NPs is five times [16] and ten times [18] higher than when using Au NPs. In polymer solar cells, adding SiO_2@Au CS NPs to the ZnO electron transport layer increased the efficiency from 3.52% to 4.20% [19]. This boost originates from the localized surface plasmon resonance effect in the core-shell structure. The silica core changed the behavior of the gold shell, which improved the electric-field distribution and enhanced light absorption.

Despite advancements in CS NPs technology, current methods for creating SiO_2@Au CS NPs face several challenges in achieving a one-step, inexpensive process that produces a uniform shell thickness and consistent structures. The widely used traditional seed-mediated growth technique often requires multiple steps and is time-consuming [20]. Additionally, it is challenging to achieve this unless the core is functionalized with amino (-NH_2) or mercapto (-SH) groups. Alternatively, complete CS NPs can be obtained by adding $HAuCl_4$ to silica multiple times [21]. Keli Wang and co-workers synthesized SiO_2@Au CS NPs using the seed growth method. They used polyethyleneimine (PEI) on a silica surface via electrostatic self-assembly to form the SiO_2@PEI NPs. Subsequently, they adsorbed 3-5 nm Au NPs on the SiO_2@PEI NPs and monodisperse SiO_2@Au CS NPs were formed within five minutes after reducing $HAuCl_4$ with hydroxylammonium chloride under the stabilization of PVP. For instance, the modified Stöber method requires surface modification of the silica core and careful control of reagent concentrations to achieve uniform gold shell thickness [22]. Similarly, the approach described in [23] involves chemical reduction followed by a modified Stöber method, which is a multistep process. Moreover, although progress has been made in developing methods for synthesizing CS NPs, including silica@gold structures, there is still room for improvement in terms of simplicity, cost-effectiveness, and precise control over shell thickness. Future research could focus on combining the strengths of the existing methods, such as the rapid sonication approach from [21], with novel templating or deposition techniques to address this unmet need in the field.

Recognizing these gaps, our study introduces a novel synthesis method that is straightforward, cost-effective, and less time- and material-intensive for producing SiO_2@Au CS NPs. To create SiO_2@Au CS NPs, a direct deposition method called the iterative hydroxylamine seeding method was utilized [24], which is both simple and cost-effective. This method requires fewer chemical materials and involves the addition of hydroxylamine and HAuCl4 four times to attain a uniform gold shell coating. Sodium citrate was also introduced into the bare silica to replace OH – with citrate ions. Au ions were then added to the SiO_2-hydroxylamine complex and reduced to Au atoms using hydroxylamine. To bond the anti-morphine antibody with the CS NPs (SiO_2@Au), ionic and hydrophobic interactions were used between the positively charged groups on the antibody surface and negatively charged surface of the SiO_2@Au CS NPs. The application of SiO_2@Au NPs as a colorimetric detector was verified by immobilizing BSA-morphine on a nitrocellulose membrane and overlaying the conjugate nanoparticles.

MATERIALS AND METHODS

Materials

Hydrochloroauric acid trihydrate ($HAuCl_4 \cdot 3H_2O$,), hydroxylammonium chloride ($NH_2OH.HCl$) and trisodium citrate dehydrate ($Na_3C_6H_5O_7 \cdot 2H_2O$) were purchased from Shanghai Chemical Co. (Shanghai, China). Phosphate buffered saline (PBS) and bovine serum albumin (BSA) were obtained from Sigma-Aldrich (Louis, MO, USA), Tris hydroxymethyl aminomethane (Tris), Tween 20, sodium azide, and Tetraethyl orthosilicate (TEOS) were purchased from Merck Schuchardt (Hohenbrunn, Germany). Bradford reagent and Nitrocellulose membrane were obtained from DNA biotech life science. Anti-morphine antibody (AM antibody) and morphine-bovine serum albumin (MOR-BSA) were provided by Artron BioResearch Inc., Canada. All other reagents, including an ammonia solution (NH_4OH, 28-30%), absolute ethanol (C_2H_5OH, 99.6%), nitric acid (HNO_3, 65% extra pure), sodium chloride (NaCl), potassium carbonate (K_2CO_3), hydrochloric acid (HCl, 37%), and deionized (DI) water were obtained from the laboratory.

Methods

Synthesis of SiO_2 nanoparticles

SiO_2 nanoparticles were synthesized using a modified Stöber method [16]. A solution of ammonia (28-30% NH_3 as NH_4OH) and ethanol (absolute and 96%) in a 2:10 v/v ratio was prepared, and tetraethyl orthosilicate (TEOS) was slowly added dropwise under vigorous stirring (Table 1). After 19 h, the reaction was considered complete, and the resulting silica nanoparticles were washed and centrifuged five times at 1500 rpm. Finally, the nanoparticles were dispersed in DI water, poured into a petri dish, and dried at room temperature.

Synthesis of SiO_2@Au core-shell nanoparticles

SiO_2@Au CS NPs were produced using a modified iterative hydroxylamine seeding technique [24]. First, the dehydrated SiO_2 NPs were sonicated in 10 ml of DI water for 10 min. These particles were subsequently mixed with trisodium citrate and agitated for 15 min to enhance their negative surface charge. Separate solutions of 80 mM hydroxylammonium chloride and gold salt (1mM, 2mM, 3mM, and 4mM) were prepared. While the SiO_2 NP/citric acid mixture was constantly stirred, 200 µL of the hydroxylammonium chloride solution was introduced dropwise over 2-3 minutes. This was followed by the gradual addition of 200 µL of gold salt solution, with this process consequent addition of $NH_2OH.HCl$ + $HAuCl_4 \cdot 3H_2O$ being repeated four times. Upon completion, the SiO_2@Au CS NPs were isolated by washing five times and centrifugation at 4°C for 20 min at 9000 rpm and then resuspended in DI water. The resulting greyish-blue hue of the solution indicates successful synthesis (Fig 1).

Characterization

The study employed a variety of analytical techniques to investigate the characteristics of SiO_2 and SiO_2@Au core-shell nanoparticles (CS NPs). Detailed imaging of the SiO_2 and SiO_2@Au CS NPs morphology was achieved through MIRA3 TESCAN field-emission scanning electron microscopy (FE-SEM) from the Czech Republic at an accelerating voltage of 15 kV. The transformation of SiO2 into SiO_2@Au CS NPs was demonstrated by a visible color change in the solution, further verified using UV-vis absorption spectroscopy with a Cecil CE 7250 Spectrophotometer in the 200-900 nm spectral range. Nanoparticle sizing employed equations by Haiss and collaborators [24], while hydrodynamic size and zeta potential measurements were taken using a particle size analyzer Scatterscope (I) (South Korea) and a Malvern ZEN 300 Zetasizer (Germany), respectively. Finally, the elemental composition of both types of nanoparticles was confirmed using energy-dispersive X-ray analysis (EDX) from Oxford Instruments, verifying the presence of the required elements.

Table 1. Synthesis conditions and particle sizes of silica nanoparticles

No.	C_2H_5OH (mL)	NH_4OH (mL)	TEOS (mL)	Yield (g)	Size by DLS (nm)
Exp. 1	10 (96%)	2.0	1.0	0.2467	325 ± 3
Exp. 2	10 (absolute)	2.0	1.0	0.2220	315 ± 2
Exp. 3	10 (absolute)	2.0	0.5	0.1676	287 ± 2
Exp. 4	10 (absolute)	2.0	0.4	0.0865	226 ± 2

(cc) BY

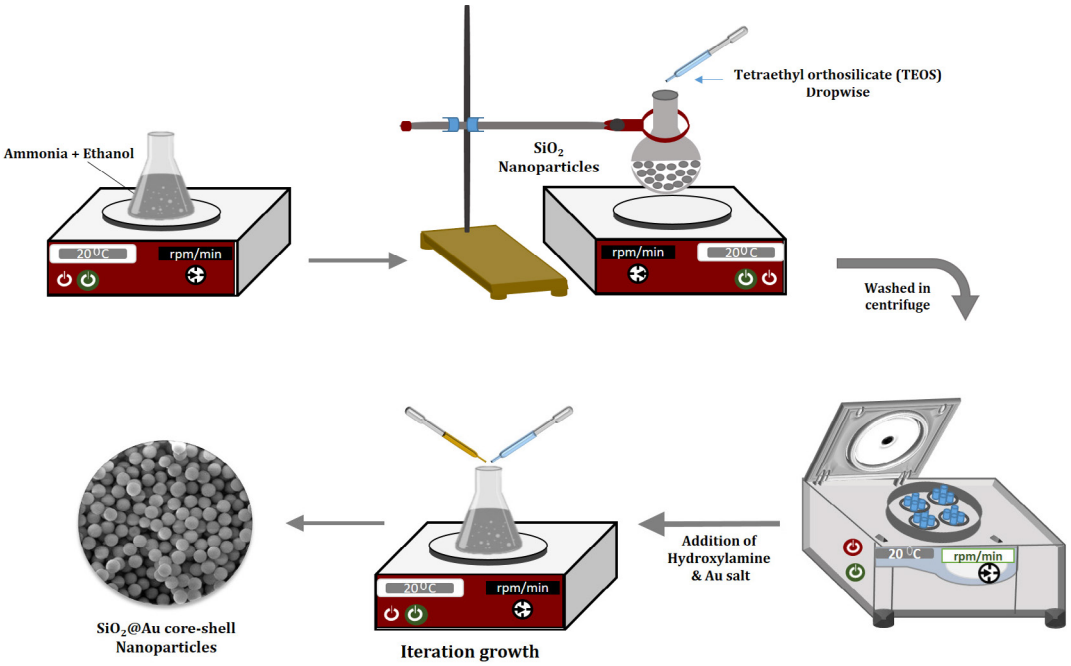


Fig. 1. Graphical abstract displaying the preparation of SiO_2 and SiO_2@Au CS NPs.

Conjugation of antibody onto the surface of nanoparticles

SiO_2@Au CS NPs were prepared based on Babaei-Afrapoli et al. [25] with a few modifications. The pH was adjusted to 8.0, and the antibody was added to the NPs solution. The mixture was stirred overnight at 4°C to allow the antibody to attach to the surface of the NPs through electrostatic interactions. The following day, 5.0% (w/v) BSA solution was added to block the uncoated areas of the NPs. The mixture was stirred for 2 h and centrifuged for 40 minutes at 10000 rpm. The resulting pellet was resuspended in a solution containing sodium borate buffer (20 mM, pH 8.0, 1.0% (w/v) BSA, and 0.1% (w/v) sodium azide). The resuspended solution was stored at 4°C until further use.

Conjugation efficiency of antibody

The efficiency of antibody binding to the SiO_2@Au CS NPs surface was measured using the Bradford assay, following the method of a previous study [25, 26]. The pH of SiO_2@Au CS NPs solution was adjusted to 8.0 and 5.0 µL of anti-morphine antibody (20.0 mg/mL) was added to it. After incubation for 20 min, the solution was centrifuged at 8000 rpm for 10 min to obtain the supernatant containing unconjugated antibodies. Therefore, 200.0 µL of the supernatant was added to 800.0 µL of Bradford solution and incubated for 15 min in darkness. Finally, the absorption (adsorption was used for physical attachment, for UV-visible absorption) of the sample was measured at 595 nm using a plate reader (Cytation, Bio Tek, USA). The following equation was used to calculate conjugation efficiency:

Conjugation efficiency % = (mass of protein used − mass of protein in suspension/mass of protein used) × 100 (Equation 1).

Performance of antibody-SiO_2@Au CS NPs

The Dot blot technique was used to evaluate the performance of the morphine anti-morphine antibody -SiO_2@Au CS NPs as a colorimetric probe. To achieve this, the small amounts of MOR-BSA (0.5 mg/mL and 1 mg/mL) and BSA (0.5 mg/mL) were added to the three pieces of the NC membranes, separately, and left to dry for 2 h. After drying, the NC membranes were soaked in block solutions (5% BSA in PBS-T) for 1 h, the block solutions were removed, and the NC membranes were left to dry for 2 h. Conjugated NPs solutions were added to each NC membrane separately and incubated for 2 h. After that, the NPs solutions were removed, and NC membranes were washed five times with PBS-T (0.05% BSA in

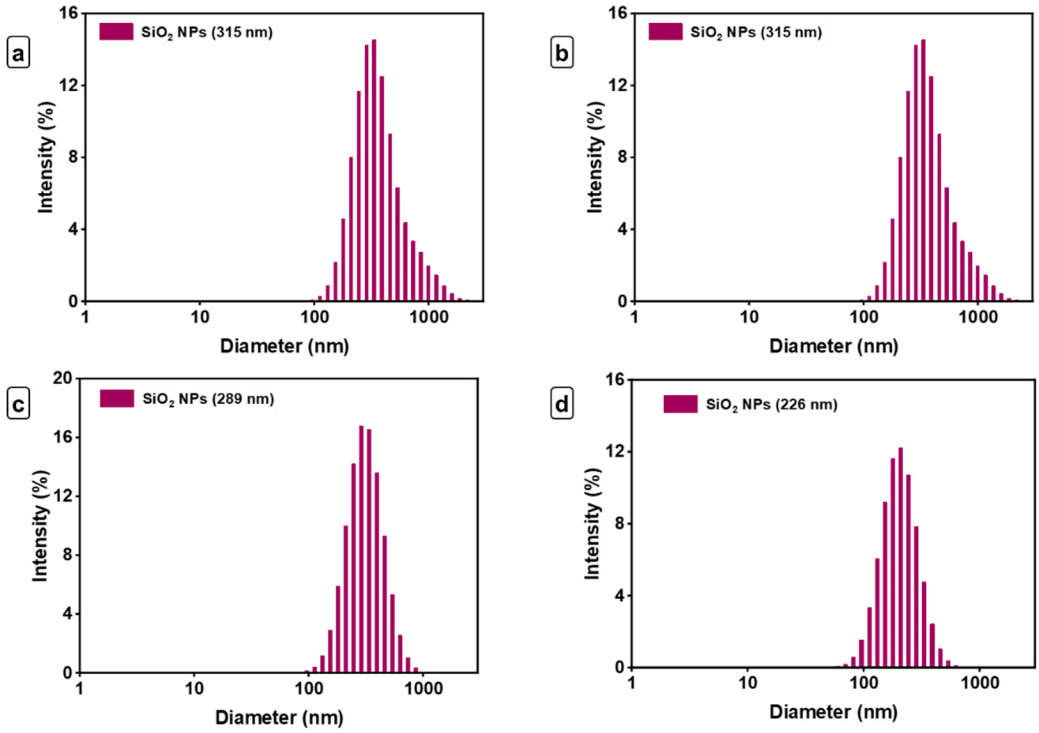


Fig. 2. (a) DLS size distributions for silica nanoparticles from four experiments, showing average hydrodynamic diameters of 325 ± 3 nm, 315 ± 2 nm, 289 ± 2 nm, and 226.2 ± 2 nm.

PBS) with a 5-minute interval between each wash. The formation of colorimetric circles on each NC membrane, arising from the interaction between AM antibody-conjugated SiO_2@Au CS NPs and MOR-BSA or BSA, was ultimately assessed.

RESULTS AND DISCUSSION

Synthesis and Characterization of SiO_2 nanoparticles

The appearance of white color in the solution was a sign of the formation of silica in the solution. To optimize the parameters involved in the synthesis of NPs, the influence of water content of the ethanol used, the concentration of TEOS on the particle size and the powder yielded after the drying process was studied (Table 1). The concentration of ammonium hydroxide (NH_4OH) was kept constant across these experiments. The average size of the particles and their size distribution were assessed by using dynamic light scattering (DLS). Larger particles measuring 325 ± 3 nm were created using 96% ethanol, whereas smaller particles of 226 ± 2 nm size were obtained with absolute ethanol. This decrease in particle size is attributed to the reduced water content in absolute ethanol, which decelerates hydrolysis and condensation during the sol-gel process, allowing for more controlled growth of the particles.

Further size reduction was achieved by decreasing TEOS volume from 1.0 mL to 0.5 mL, resulting in particles measuring 289 ± 2 nm in diameter. This is consistent with the understanding that lower precursor concentrations limit reactant availability, reducing particle growth rate. Further reducing the amount of TEOS in combination with absolute ethanol resulted in smaller particle sizes (226 ± 2) (Fig. 2d). The histogram presenting the distribution of the particle diameters from SEM micrographs of SiO_2 NPs (Exp 4) in Fig 3b revealed that the average particle size is 178 nm. However, the 226 nm average suggests that the hydrodynamic size is approximately 48 nm larger than the DLS size because it measures the particle as it behaves in solution while SEM measures the solid SiO_2 NPs core in a dry and static state.

The successful synthesis of silica nanoparticles was confirmed by FESEM, revealing spherical nanoparticles with excellent monodispersity. The particles exhibit uniform spherical morphology, consistent size distribution, and well-defined boundaries (Fig. 3a-b). Fig. 3c shows the EDX

(cc) BY

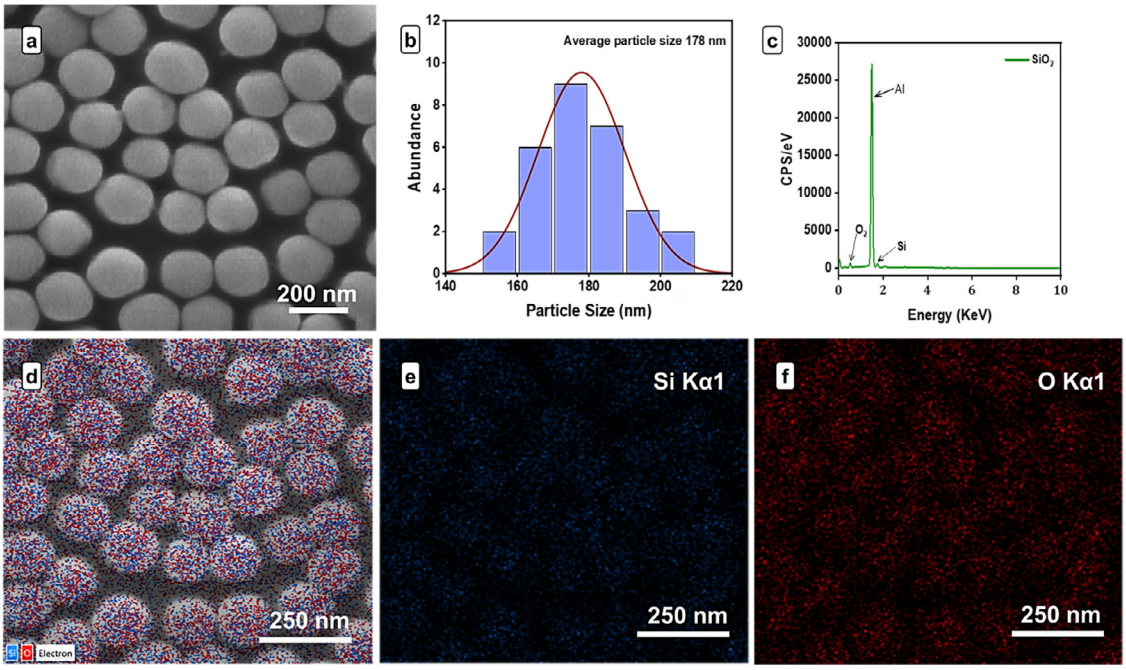


Fig. 3. (a) SEM images showing the morphology of the SiO_2 NPs, (b) Particle size distribution histogram derived from SEM micrographs of SiO_2 NPs (Experiment 4), (c) Representative mapping image indicating a particle size of 178 nm, (d-f) EDX elemental maps illustrate the spatial distribution of Si and O within the NPs.

spectrum with distinct peaks for silicon (~1.7 keV) and oxygen (~0.5 keV), confirming the presence of SiO_2. Fig. 3d presents a composite elemental map, while Figs. 3e and 3f display individual maps of silicon and oxygen, respectively.

The EDX result shows a higher atomic percentage of oxygen (77.47 %) compared to silicon (22.53 %). The O: Si atomic ratio is ~3.44, which deviates from the ideal stoichiometry of SiO_2, where oxygen and silicon should be present at ~66.6% and ~33.3% atomic percentages, respectively. This is common because of the surface adsorbates that can contribute to the oxygen signal.

The zeta potential measurements revealed that the smaller silica nanoparticles exhibited a zeta potential of -6.21 mV. The negative surface charge is typical of silica particles in aqueous or alcoholic dispersions due to deprotonated silanol groups on their surfaces.

Characterization of core-shell nanoparticles

Synthesis parameters and respective sizes of SiO_2@Au CS NPs are summarized in Table 2. Three different concentrations of gold salt solution were used while keeping the concentrations of SiO_2 NPs and $NH_2OH{\cdot}HCl$ as the linker/reducing agent constant. The SiO_2 NPs served as the core material and $NH_2OH{\cdot}HCl$ as the reducing agent to facilitate gold shell formation. Gold concentration varied across experiments (1, 2, and 3 mM) to control the amount of gold available for shell growth. Moreover, increasing the concentration of gold salt solution resulted in formation of CS NPs with an average hydrodynamic diameter of 274 ± 7 nm, 284 ± 8 nm and 291 ± 5 nm, respectively. The effect of gold salt concentration on nanoparticle size clearly demonstrates that increasing the concentration of gold salt solution led to a systematic increase in the particle size of the resulting SiO_2@Au CS NPs. This can be attributed to the progressive thickening of the gold shell around the silica core as more gold ions are reduced and deposited onto the nanoparticle surface.

SiO_2@Au CS NPs exhibited characteristic plasmonic peak in UV-vis absorption spectra (Figure 4). The black curve represents pure SiO_2 NPs, showing minimal absorption over the entire visible and near-infrared range (400-900 nm). This confirms that the silica core contributes negligibly to the optical properties, making it an ideal dielectric core material. SiO_2@Au (1 mM Gold) exhibits a broad absorption band centered around 650-700

CC BY

Table 2. Results of DLS size measurement of SiO_2@Au core-shell nanoparticles synthesized using three different concentrations of gold on 226 ± 2 nm silica core.

No.	SiO_2 NPs (mg/mL)	$NH_2OH.HCl$ (mM)	Gold (mM)	Size by DLS (nm)
Exp. 5	10	80	1	274 ± 7
Exp. 6	10	80	2	284 ± 8
Exp. 7	10	80	3	291 ± 5

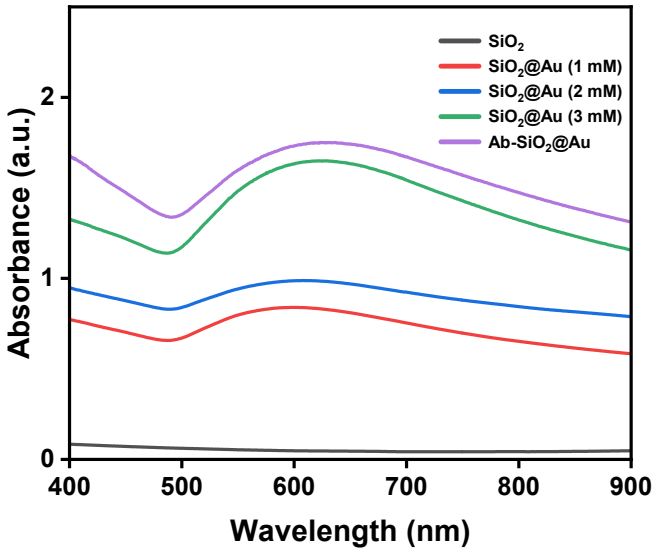


Fig. 4. UV-vis absorption spectrum showing the absorbance curve of bare SiO_2, SiO_2@Au CS NPs and Ab-SiO_2@Au CS NPs

nm with moderate intensity. This represents the fundamental dipolar surface plasmon resonance of the thin gold shell. SiO_2@Au (2 mM Gold), showed similar spectral characteristics but with slightly modified intensity, indicating shell growth while maintaining the core-shell architecture. Additionally, SiO_2@Au (3 mM Gold), demonstrated increased absorption intensity and broader spectral features, suggesting thicker gold shell formation with enhanced plasmonic coupling. SiO_2@Au (1 mM Gold) was used for the conjugation of antibody. The conjugation of anti-morphine antibody did not affect the UV-visible absorption spectrum of the core-shell structure confirming the integrity of the sample.

The DLS data show the hydrodynamic size distributions of SiO_2@Au CS NPs synthesized with gold salt concentrations (1, 2, and 3 mM), it indicates that the gold shell growth led to increasing the size from 226 ± 2 nm to 274 ± 7 nm, 284 ± 8 nm, and 291 ± 5 nm, suggesting a gold shell thickness of approximately 48 ± 7 nm, 58 ± 8 nm, and 65 ± 5 nm, respectively (Fig. 5a-c). The size distributions are narrow for all samples, indicating uniform and monodisperse nanoparticle populations. The systematic increase in the mean diameter confirms that increasing the amount of gold precursors results in thicker gold shells around the silica core (Table 2).

The SEM micrographs and size distribution (Fig. 6a-b) and associated elemental mapping (Fig. 6d-h) offer a comprehensive morphological and compositional characterization of SiO_2@Au CS NPs. Sample in Fig 6a display highly uniform, spherical particles with smooth surfaces. The particles are well-dispersed and non-aggregated, indicating good colloidal stability and successful control of synthesis conditions. The monodispersity and uniformity are visually confirmed, supporting the DLS findings of narrow size distributions.

Figure 6b shows histograms of particle size distributions obtained from SEM micrographs of the SiO_2@Au CSNPs, with average diameters of 182 nm. However, the corresponding DLS measurements of 291 ± 5 nm are approximately 101 nm larger. This difference arises because DLS

(cc) BY

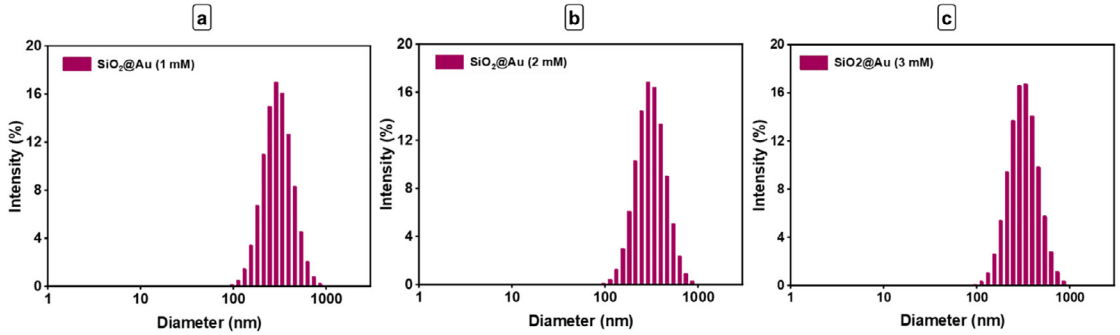


Fig. 5. (a–c) DLS size distributions of SiO_2@Au CSNPs at 1 mM, 2 mM, and 3 mM precursor concentrations, yielding average hydrodynamic diameters of 274 ± 7 nm, 284 ± 8 nm, and 291 ± 5 nm, respectively.

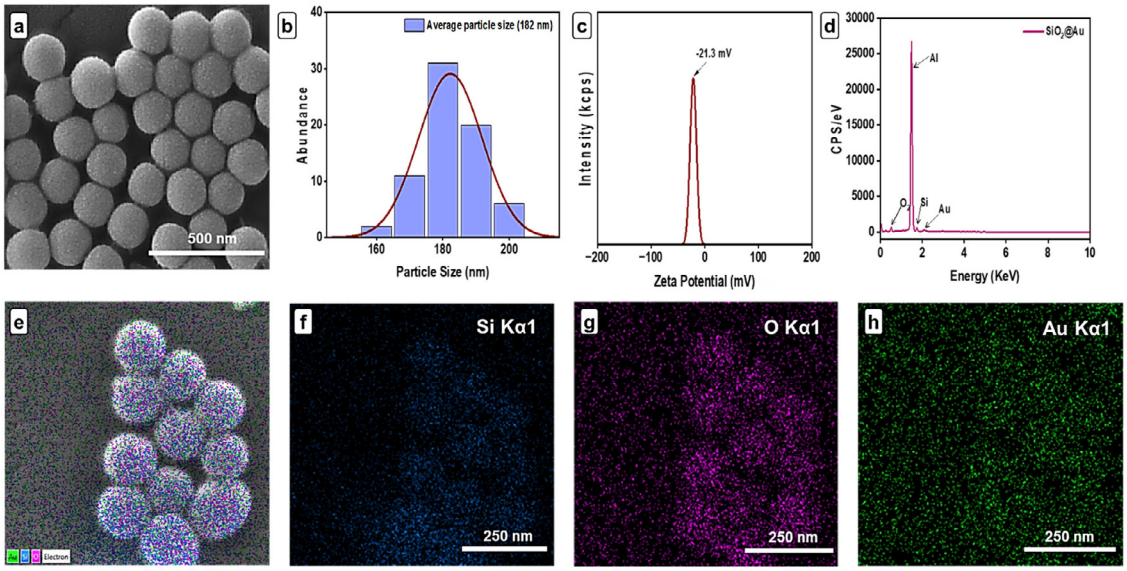


Fig. 6. (a) SEM images showing the morphology of the SiO_2@Au CS NPs. (b) Particle size distribution histogram derived from SEM micrographs of SiO_2@Au CS NPs. (c) Zeta potential measurement of the SiO_2 NPs (-21.3 mV). (d) Representative mapping image indicating a particle size of 182 nm, (e-h) EDX elemental mapping of Si, O and Au.

measures the particles in their solvated, dynamic state, capturing the influence of the surrounding solvation layer and any surface-bound species, whereas SEM reflects the dry, static dimensions of the solid SiO_2 core–shell structures.

Figure 6c presents the zeta potential measurement for the SiO_2@Au nanoparticles synthesized with 3 mM gold salt, showing a value of -21.3 mV. Zeta potential quantifies the surface charge of nanoparticles in suspension, which directly influences colloidal stability. A value of -21.3 mV suggests moderately good stability: the negative surface charge results from the presence of citrate ions on the surface of Au NPs decorating the surface. While absolute values above ± 30 mV are often considered highly stable, values in the range of ± 20 to ± 30 mV generally indicate sufficient electrostatic repulsion to prevent rapid aggregation under typical storage and handling conditions.

EDX spectrum of the 3 mM gold sample (291 ± 5 nm) in Fig. 6d shows distinct peaks for silicon (Si), oxygen (O), and gold (Au), confirming the core-shell elemental composition. Composite mapping image. Fig. 6e overlays elemental distributions and individual elemental maps for Si (blue), O (magenta), and Au (green) for the 3 mM gold sample in Fig 6f-h. Si and O elements are localized to the core, confirming the presence of silica at the center of each particle, while Au element was evenly distributed as a shell around each core,

CC BY

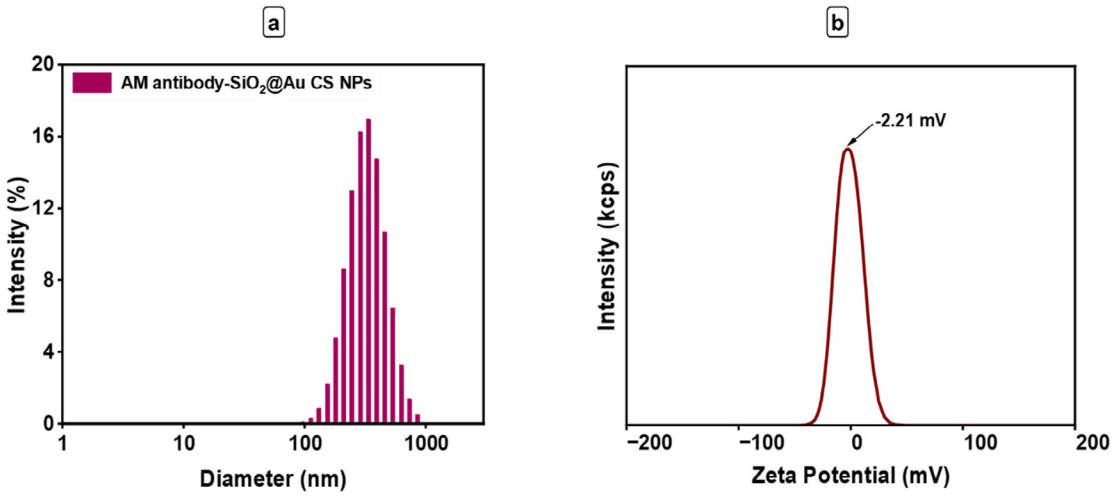


Fig. 7. DLS results of conjugated nanoparticles (301 ± 3 nm) and zeta potential of conjugated nanoparticles (-2.21 mV).

confirming uniform gold coating. The SEM and elemental mapping conclusively demonstrate that the particles are SiO_2 cores uniformly coated with a gold shell. The systematic increase in particle size with increasing gold precursor concentration directly visualizes the tunability of the decoration, a key parameter for tailoring optical and catalytic properties making it suitable for applications such as drug delivery, imaging, biosensing, and catalysis.

Conjugation of antibody onto the surface of nanoparticles

The size of the AM antibody-SiO_2@Au CS NPs was 10 ± 8 nm, with a recorded zeta potential of -2.21 mV. DLS results indicated a notable increase in size from 291 ± 5 nm to 301 ± 3 nm (Fig. 7a). The increase in hydrodynamic diameter compared to unconjugated SiO_2@Au CS NPs (which ranged from 226 ± 7 nm to 291 ± 5 nm depending on gold shell thickness) confirms successful surface conjugation with anti-morphine antibodies. The size increase is consistent with the addition of a biomolecular corona (antibody layer) surrounding each nanoparticle, which contributes to the hydrodynamic radius measured by DLS.

The zeta potential value -2.21 mV (Fig. 7b) is close to neutral, indicating a significant reduction in surface charge compared to the unconjugated SiO_2@Au CS NPs, which had a zeta potential of -21.3 mV for the thickest gold shell. This reduction is expected after antibody conjugation, as the protein layer can mask the original surface charge and introduce new surface groups, often leading to a zeta potential closer to zero. A near-neutral zeta potential can reduce electrostatic repulsion between particles, potentially increasing the risk of aggregation in some conditions. However, stability may still be maintained by steric effects from the antibody layer [27].

Binding efficiency of antibody by Bradford assay

To evaluate the binding efficiency of the antibody to CS NPs, a Bradford assay was performed. The amount of conjugated antibody on the surface of the SiO_2@Au NPs was quantified at 280 nm by UV-visible spectroscopy. Binding efficiency was calculated by subtracting the initial unbound antibody concentration (blank) from the total amount added. Uniformly sized particles, measuring 301 ± 3 nm, exhibited a binding capacity of 99%.

Dot blot immunoassay

A dot blot assay was conducted to evaluate the performance of the SiO_2@Au CS NPs as a colorimetric probe and the specificity of the anti-morphine antibody to detect morphine. The observed color intensity was directly proportional to the quantity of MOR-BSA applied and the concentration of conjugated anti-morphine antibody-SiO_2@Au CS NPs. Increased concentrations of anti-morphine antibody-SiO_2@Au CS NPs combined with lower concentrations of MOR-BSA facilitated significant color development. Conversely, challenges arose in visually assessing results with a high concentration of MOR-BSA (1 mg/mL), which resulted in

(cc) BY

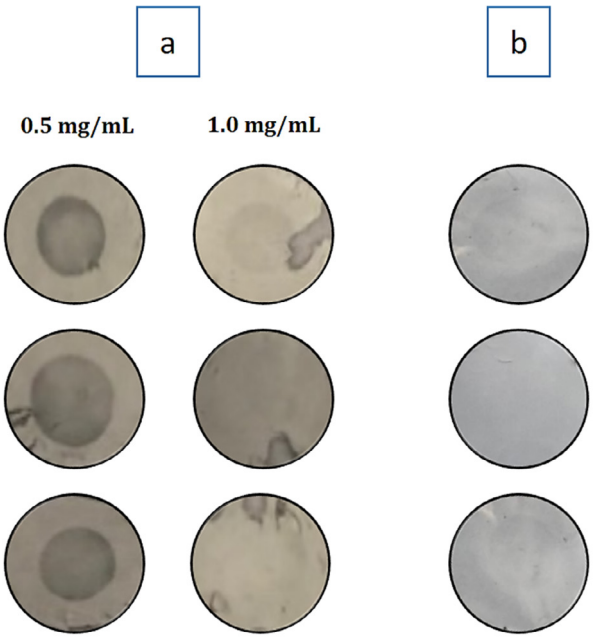


Fig. 8. Dot blot assay: a) nitrocellulose membrane containing 0.5 and 1.0 mg/mL MOR-BSA incubated with conjugated nanoparticles, b) nitrocellulose membrane containing 0.5 mg/mL BSA incubated with conjugated nanoparticles.

reduced color intensity of anti-morphine antibody-SiO_2@Au CS NPs, even after 30 min. In contrast, a lower concentration of MOR-BSA (0.5 mg/mL) and a higher intensity of anti-morphine antibody-SiO_2@Au CS NPs resulted in an effective visual assessment within 3-4 minutes. Additionally, no coloration was observed on the NC membrane containing only BSA, suggesting that the anti-morphine antibody exhibits specific interactions with morphine molecules. This experiment was repeated thrice, as shown in Fig. 8.

The research findings indicate that NPs with multiple phases that include inorganic components outperform their single-phase counterparts in various applications. Notably, Alkurdi et al. research highlights the superior heat transfer capabilities of gold-silica core-shell nanoparticles when interacting with liquid water, surpassing those of uniform gold nanoparticles of equivalent size. This improvement in heat transfer efficiency is primarily due to the effective interfacial interaction between the electrons in the metal and the phonons in the silica [28].

Furthermore, our project successfully validated a critical design principle: size matters when you're building a nanoparticle detection system. We observed that our SiO2@Au core-shell nanoparticles exhibited higher antibody adsorption efficiency nearly 99%, a direct benefit of their larger size, which offers more surface area for attachment. This confirms what others have reported, where increased nanoparticle size has been shown to enhance antibody loading capacity by providing more available surface area and improving the proportion of antibodies that retain antigen-binding activity. Babaei *et al.* observed a clear trend where the adsorption efficiency of antibody molecules on the surface of Au NPs rises from 21% ± 3.75, 44% ± 2.46, and 50% ± 6.15 for sizes 12 ± 1.08, 32 ± 1.46, and 64 ± 2.24 nm, respectively. They indicated that this occurs because the larger NPs offer increased surface area for the adsorption of antibody molecules [25]. Similarly, other studies corroborate this, noting that as Au NP diameter increases, the percentage of antibody valences that retain their antigen-binding capabilities rises from 17% to 34% [29]. While conventional methods, such as that by Davatgaran *et al.*, which used direct adsorption on single-phase Au NPs, achieved approximately 60% antibody adhesion [30].

The silica-gold core-shell structure is our deliberate advantage. It gives us the stability needed for a reliable assay, plus the enhanced conjugation efficiency required for high sensitivity. In essence, we've optimized the particle's physical dimensions to maximize its functional utility, creating a stronger foundation for our diagnostic platform.

CONCLUSION

A straightforward and reliable technique was developed to fabricate SiO_2@Au CS NPs in a single step. Compared with other synthesis methods, this approach is more efficient because of its reduced material usage and shorter processing time. This method produced a uniform and spherical CS NPs shape, as confirmed by EDX analysis. An antibody was successfully attached to nanoparticles via ionic and hydrophobic interactions, resulting in remarkably high binding efficiency. Our research has shown that morphine detection is achievable in less than 5 min, and an antibody concentration as low as 20 µg/mL is adequate for optical testing.

CONFLICTS OF INTEREST

No potential conflict of interest was reported by the authors.

ACKNOWLEDGEMENT

This work was fully funded by Tehran University of Medical Science & Health Services (grant No. 1403-1-148-71601.

REFERENCES

1. Chen CH, et al. Nanomaterial-based adsorbents and optical sensors for illicit drug analysis. J Food Drug Anal. 2020;28(4):654-676. https://doi.org/10.38212/2224-6614.1137
2. Smith MT, et al. Analgesic opioid ligand discovery based on nonmorphinan scaffolds derived from natural sources. J Med Chem. 2022;65(3):1612-1661. https://doi.org/10.1021/acs.jmedchem.0c01915
3. Pashapour S, Soltaninejad K. Morphine Analysis in Biological Samples: A Systematic Review. Pharm Anal Acta. 2024;13(3):1-15.
4. Biancuzzi H, et al. Opioid misuse: a review of the main issues, challenges, and strategies. Int J Environ Res Public Health. 2022;19(18):11754. https://doi.org/10.3390/ijerph191811754
5. Igharo O, et al. Clinical laboratory techniques for detecting drugs of abuse: Feasibility in developing nations. Afr J Health Sci. 2024;23(2):339-348. https://doi.org/10.4314/sa.v23i2.31
6. Syedmoradi L, Norton ML, Omidfar K. Point-of-care cancer diagnostic devices: From academic research to clinical translation. Talanta. 2021;225:122002. https://doi.org/10.1016/j.talanta.2020.122002
7. Zhang Z, et al. Plasmonic colorimetric sensors based on etching and growth of noble metal nanoparticles: Strategies and applications. Biosens Bioelectron. 2018;114:52-65. https://doi.org/10.1016/j.bios.2018.05.015
8. Afrapoli ZB, et al. Design principles of paper-based sensors. In: Paper-Based Optical Chemosensors. Elsevier; 2025. p. 199-264. https://doi.org/10.1016/B978-0-443-13356-5.00005-7
9. Luo L, et al. Gold-loaded mesoporous organosilica-silica core-shell nanoparticles as catalytic nanoreactors. Eur J Inorg Chem. 2020;2020(41):3967-3976. https://doi.org/10.1002/ejic.202000691
10. Szabat H, et al. Shell tailoring of core-shell nanoparticles for heterogeneous catalysis. Colloids Surf A Physicochem Eng Asp. 2021;128:107055. https://doi.org/10.1016/j.elecom.2021.107055
11. Zhang Z. Research progress of gold core-shell structured nanoparticles in tumor therapy. J Phys Conf Ser. 2020;1549:032056. https://doi.org/10.1088/1742-6596/1650/3/032056
12. Nandanwar R, Singh P, Haque FZ. Synthesis and properties of silica nanoparticles by sol-gel method for the application in green chemistry. Mater Sci Res India. 2013;10(1):85-92.
13. Rahman IA, Padavettan V. Synthesis of silica nanoparticles by sol-gel: size-dependent properties, surface modification, and applications in silica-polymer nanocomposites-a review. J Nanomater. 2012;2012:132424. https://doi.org/10.1155/2012/132424
14. Singh LP, et al. Sol-gel processing of silica nanoparticles and their applications. Adv Colloid Interface Sci. 2014;214:17-37. https://doi.org/10.1016/j.cis.2014.10.007
15. Deiminiat B, et al. A novel electrochemical imprinted sensor for acetylsalicylic acid based on polypyrrole, sol-gel and SiO2@Au core-shell nanoparticles. Sens Actuators B Chem. 2017;244:785-795. https://doi.org/10.1016/j.snb.2017.01.059
16. Daware K, et al. Detection of toxic metal ions Pb2+ in water using SiO2@Au core-shell nanostructures: A simple technique for water quality monitoring. Spectrochim Acta A Mol Biomol Spectrosc. 2019;732:136635. https://doi.org/10.1016/j.cplett.2019.136635
17. Amani N, Azizkandi N. Investigation of Core-Shell Nanoparticle in a Confined Space of a Periodic Substrate Based on SERS. Opt Spectrosc. 2020;54(8):863-868. https://doi.org/10.1134/S1063782620080047
18. Thatai S, et al. Trace colorimetric detection of Pb2+ using plasmonic gold nanoparticles and silica-gold nanocomposites. Microchem J. 2016;124:104-110. https://doi.org/10.1016/j.microc.2015.07.006
19. Chen X, Yan L. Application of Au, SiO2@Au, and Au@SiO2 nanoparticles in PTB7:PC71BM polymer solar cells. J Mater Sci Mater Electron. 2017;28:13698-13704. https://doi.org/10.1007/s10854-017-7213-y
20. Wu R, et al. A comprehensive Review: The approach for fabrication of Core/Shell Au nanocomposite and Modification, Properties, applications of Au NPs. Microchem J. 2024;199:101824. https://doi.org/10.1016/j.jscs.2024.101824
21. Wang K, et al. Facile synthesis of high-performance SiO2@Au core-shell nanoparticles with high SERS activity. RSC Adv. 2018;8(54):30825-30831. https://doi.org/10.1039/C8RA05213A
22. Nghiem THL, et al. Preparation and characterization of silica-gold core-shell nanoparticles. J Nanopart Res. 2013;15:1-9. https://doi.org/10.1007/s11051-013-2091-6
23. Raj S, Rai P, Yu YT. Pulse electrophoresis deposition of Ag@SiO2 core-shell nanoparticles on FTO substrate. Mater Lett. 2014;117:116-119. https://doi.org/10.1016/j.matlet.2013.11.123
24. Lyon JL, et al. Synthesis of Fe oxide core/Au shell nanoparticles by iterative hydroxylamine seeding. Nano Lett. 2004;4(4):719-723. https://doi.org/10.1021/nl035253f
25. Babaei-Afrapoli Z, et al. Evaluating gold nanoparticles

CC BY

parameters in competitive immunochromatographic assay via dot blot and Bradford assay as new approaches. Anal Biochem. 2021;170:106525. https://doi.org/10.1016/j.microc.2021.106525

26. Gavanji K, et al. Determination of Morphine Using Carboxylated Multiwalled Carbon Nanotubes (MWCNTs) as the Label for an Immunochromatographic Assay (ICA). Anal Lett. 2024;57(17):2916-2926. https://doi.org/10.1080/00032719.2024.2307459
27. Rohani Bastami T, Bayat M, Paolesse R. Naked-eye detection of morphine by Au@Ag nanoparticles-based colorimetric chemosensors. Sensors (Basel). 2022;22(5):2072. https://doi.org/10.3390/s22052072
28. Alkurdi A, et al. Enhanced heat transfer with metal-dielectric core-shell nanoparticles. Phys Rev Appl. 2020;13(3):034036. https://doi.org/10.1103/PhysRevApplied.13.034036
29. Sotnikov DV, et al. Retention of activity by antibodies immobilized on gold nanoparticles of different sizes: Fluorometric method of determination and comparative evaluation. Nanomaterials (Basel). 2021;11(11):3117. https://doi.org/10.3390/nano11113117
30. Davatgaran Taghipour Y, Kharrazi S, Amini SM. Antibody conjugated gold nanoparticles for detection of small amounts of antigen based on surface plasmon resonance (SPR) spectra. Nanomed Res J. 2018;3(2):102-108.

(cc) BY